TRANSFORMATION STRAIN AND TEXTURE EVOLUTION DURING DIFFUSIONAL PHASE TRANSFORMATION OF LOW ALLOY STEELS STUDIED BY NEUTRON DIFFRACTION

P.G. Xu[1,2], Y. Tomota[2], S.C. Vogel[3], T. Suzuki[2], M. Yonemura[2] and T. Kamiyama[4]

[1]Quantum Beam Science Directorate, Japan Atomic Energy Agency, Ibaraki, 319-1195, Japan
[2]Graduate School of Science and Engineering, Ibaraki University, Ibaraki, 316-8511, Japan
[3]Los Alamos Neutron Science Center, Los Alamos National Laboratory, NM 87545, USA
[4]Institute of Materials Structure Science, High Energy Accelerator Research Organization, Japan

Abstract. The ferrite-to-austenite transformation during heating and the austenite-to-ferrite transformation during cooling were *in situ* investigated by KEK/SIRIUS and LANSCE/HIPPO neutron diffractometers under the stress-free condition. The deviation of ferrite lattice parameter from the linear thermal expansion and contraction during heating and cooling suggested the compressive strain occurred in ferrite phase. The texture memory effect between the cold compression texture of initial martensite and the final texture of ferrite after $\alpha \rightarrow \gamma \rightarrow \alpha$ phase transformation was interrupted by the static recrystallization of martensite during step-by-step heating, revealing that the occurrence of texture memory effect was not directly related to the deformation stored energy but related to the transformation strain and the strong variant selection for nucleation.

1. INTRODUCTION

As typical diffusional phase transformations, the ferrite-to-austenite and the austenite-to-ferrite transformations in low alloy steels have been investigated widely, including the orientation relationships and transformation textures. The parent and transformed phases have been analysed with Bain, Kurdjumov-Sachs, and Nishiyama-Wassermann orientation relationships, where the texture memory effect related to variant selection has been found to take place in the transformation textures [1-4]. However, the explanations about variant selection between the parent phase and the transformed phase are still under argument. Butron-Guillen *et al.* combined the residual stress/strain, the slip activity with the austenite grain morphology to explain the variant selections during the transformation of deformed austenite [5]. Bruckner *et al.* associated it with the residual stress and crystallographic constrains [6], Humbert *et al.* ascribed it to the elastic anisotropy of parent austenite [7] and Kestens *et al* claimed the variant with a minimized elastic strain energy was selected among different Bain variants [8]. Though the phase stress/strain between mother and newly transformed phases may provide direct data in modeling the variant selection, no quantitative measurement of phase stress/strain during diffusional phase transformations at high temperature has been reported because these transformations involve evident composition diffusion and the solute concentration change in austenite.

The *in situ* neutron diffraction is well known as a powerful material characterization tool to evaluate

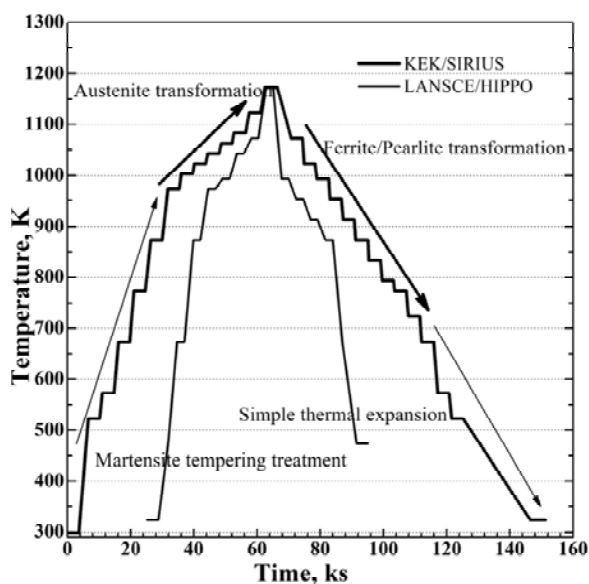Corresponding author: P.G. Xu, e-mail: xu.pingguang@jaea.go.jp

Fig. 1. Temperature history of low alloy steel for neutron diffraction experiments.

the microstructure evolution in bulk specimens under various environments [9,10]. Onink *et al* measured the lattice parameters of ferrite and austenite as functions of temperature in Fe-C alloys [11]. Te Velthuis *et al.* reported the lattice expansion coefficients of ferrite and austenite in Fe-Cu and Fe-Co binary alloys and evaluated the phase strains during the phase transformation in case of no change in chemical compositions of constituent phases [12]. Xu *et al.* compared the lattice parameters of ferrite and austenite in low alloy steels during ferrite transformation with and without prior austenite deformation and found that the deviations from the linear thermal contraction occurred both in ferrite and austenite during step-by-step cooling [13]. However, considering the angle dispersive neutron diffraction profiles are usually with a low signal/noise

(S/N) ratio due to the weak beam flux and the short profile collecting time, the lattice parameters of austenite and ferrite is necessary to be measured precisely by time-of-flight (TOF) neutron diffraction before evaluating the phase strains in diffusional transformation.

In this paper, the microstructure evolution in the austenite transformation, the ferrite transformation and the thermal expansion behavior of C-Mn low-alloy steel was *in situ* investigated by neutron diffraction and the texture evolution of cold compressed specimen during step-by-step heating and cooling was also measured by neutron diffraction.

2. EXPERIMENTAL PROCEDURES

The world-first spallation neutron source for neutron scattering experiments was constructed at KEK/KENS in Japan (5 kW). The J-PARC neutron source was established to replace the KENS where the neutron beam intensity of the J-PARC was expected to become 200 times higher than that of the KENS. As a primitive trial to measure reverse and forward austenite-ferrite phase transformation at KENS/SIRIUS neutron diffractometer, an as-quenched 2Mn-0.2C martensite steel was employed as the starting material in order to avoid the influence of heterogeneity in microstructure and chemical composition distribution. The columnar specimen with 7 mm in diameter and 48 mm in length was inserted in a $\varnothing$ 8 mm vanadium tube to allow free expansion and contraction, and it was heated/cooled in a specified vacuum furnace kept at 2.6×10^{-4} Pa within a temperature error about ±0.5K. The temperature history was shown in Fig. 1. The TOF data acquisition time of 3.6 ks was statistically sufficient using back scattering neutron with the time focus-
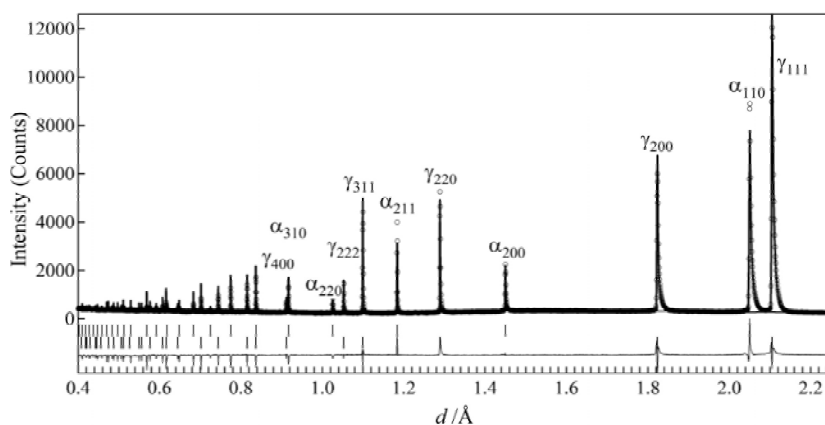

Fig. 2. Rietveld analysis of the neutron diffraction spectrum obtained in the dual phase region at 1043K during heating.
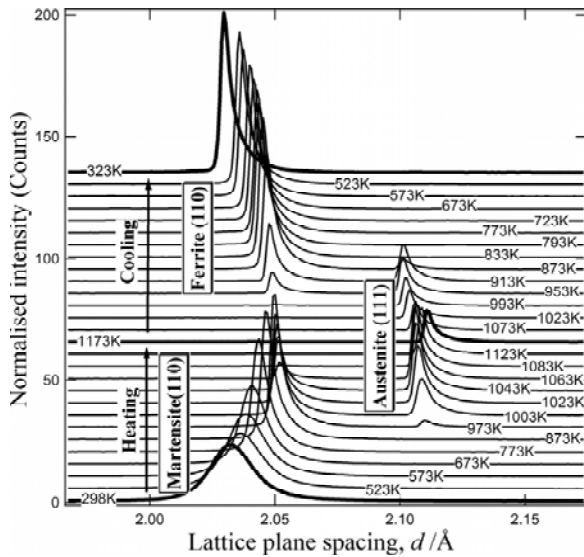
Fig. 3. Changes in neutron diffraction profiles during heating and cooling.
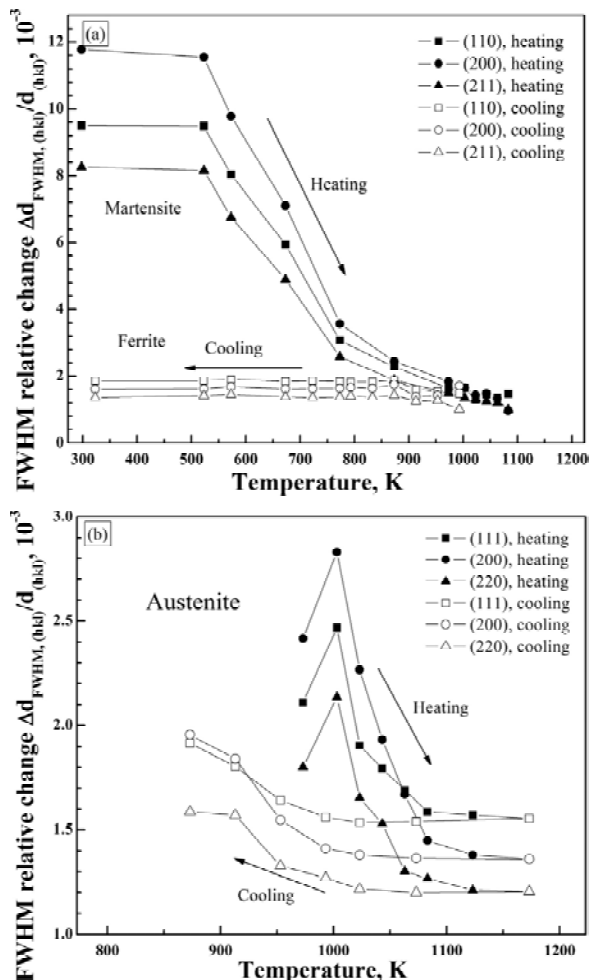

Fig. 4. Changes in full width at half maximum (FWHM) of ferrite/martensite (a) and austenite (b) in investigated low-alloy steel during heating and cooling

ing method. Because of long data acquisition time, the obtained results mean nearly equilibrium phase

condition. The whole-pattern Rietveld refinement of neutron diffraction profiles were carried out by using RIETAN-2001T software [14,15] to analyze the austenite transformation, ferrite transformation and thermal expansion behavior, as illustrated in Fig. 2.

HIPPO neutron diffractometer at Los Alamos Neutron Science Center is a general-purpose time-of-flight energy dispersive neutron diffractometer, equipped with 50 detector panels covering $2\theta = 150°$, 90°, 40°, 20°, and 10°. The 2Mn-0.2C columnar specimens with 6 mm in diameter and 6 mm in length were 50% cold compressed to get a typical starting texture. The temperature history for the *in situ* neutron diffraction under the condition of free expansion was also summarized shown in Fig. 1. In this experiment, only $2\theta = 150°$, 90°, 40° detector panels were used because of the low stereographic angle resolution of low-angle detectors. At each temperature, the total 120 time-of-flight neutron spectra obtained through $\omega = 0°$, 45°, 67.5°, 90° sample rotation during 2.4 ks acquisition were Rietveld analyzed using the MAUD software [17] with the E-WIMV discrete algorithm based texture analysis method at a discrete ODF (orientation distribution function) space cell size of 10°.

3. RESULTS AND DISCUSSION

3.1. Microstructure evolution

Fig. 3 shows the change in (110) ferrite (or martensite) and (111) austenite diffraction profiles during heating and cooling. The shift of austenite (111) and ferrite (110), and the change in their diffraction intensity during heating and cooling are clearly observed. Fig. 4 exhibits the relative change in full width at half maximum (FWHM) of martensite/ferrite and austenite, by single peak fitting with the combination of Pseudo-Voigt function and Gaussian/ exponential functions. At 298K, the starting microstructure is martensite (bct), so that the FWHM is much larger than all other cases. During heating, the tempering of martensite takes place accompanying cementite precipitation, and the FWHM becomes smaller due to decreasing of tetragonality of bct martensite. The ferrite peak begins to weaken at 973K and disappears at 1083K due to the initiation and the completion of austenite transformation, respectively. During specimen cooling, the ferrite (110) peak begins to appear at about 973K. In the single phase ferrite region, the maximum intensity of ferrite peaks increases gradually during cooling due to the temperature effect of neutron scattering but the FWHM of ferrite peaks shows little change. On the other hand, the FWHM of austenite peaks de-
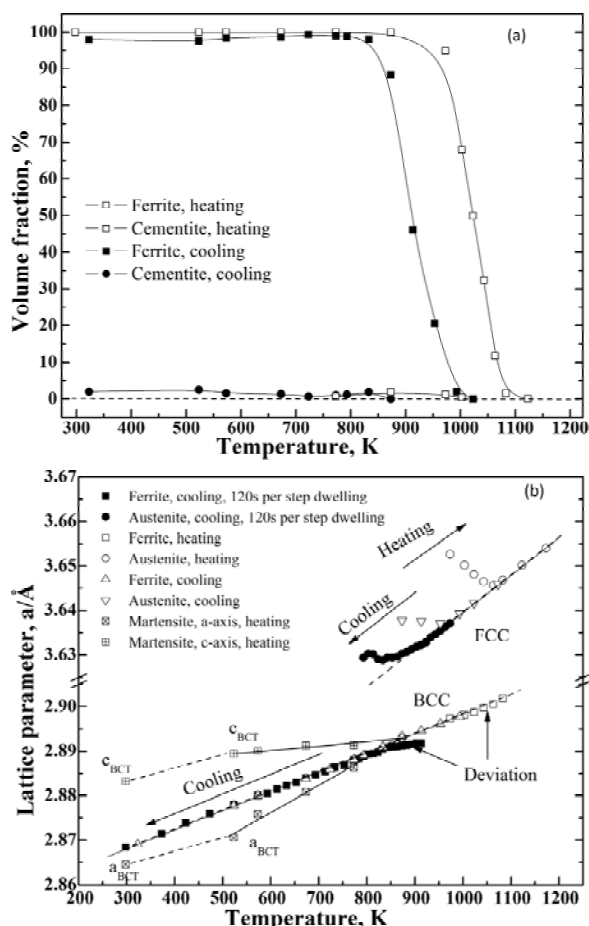
Fig. 5. Changes in volume fractions of ferrite and cementite (a) and lattice parameters of martensite/ferrite and austenite (b) of component phases in the investigated low-alloy steel during heating and cooling, obtained by Rietveld refinement.

creases with increasing of austenite amount during heating and increases with decreasing of austenite amount during cooling. In addition, the austenite and the ferrite both show that the relative FWHM change of {200} peak is more sensitive to microstructure evolution than those of other peaks.

Since the specimen was allowed to free expansion and the measuring time interval was long enough, some quantitative data about phase transformation were obtained. Fig. 5 plots the volume fractions and the lattice parameters as a function of temperature. During heating, the axial ratio c/a of martensite lattice shows little change from room temperature to 523K and then decreases linearly from 523K (c/a=1.0066) to 873K (bcc). The martensite was tempered to precipitate cementite and then austenite initiated from the cementite particles. Hence, the carbon enrichment occurs in the austenite at the beginning of austenite

transformation. During cooling, the cementite appears as a lamellar constituent phase of pearlite during pearlite transformation of carbon-enriched austenite.

Moreover, nearly linear thermal expansion is found both in single phase ferrite and in single phase austenite (Fig. 5b). The deviation from this linear relationship in dual phase region stems from above carbon enrichment in austenite and elastic strains (stresses) due to internal stress. That is to say, the lattice parameter of austenite is dependent on thermal expansion (or contraction), carbon concentration and internal stress caused by the misfit strains due to the transformation strain and the difference of thermal expansion rate between ferrite and austenite. The deviation of austenite lattice parameter from the lineal thermal expansion is more evident during heating than that during cooling in Fig. 5b confirms that the higher carbon concentration in austenite occurs at the beginning of austenite transformation than at the end of ferrite transformation. It is well known that the critical carbon concentration in austenite of Fe-C steels is 0.77 mass% for the initiation of pearlite lamellar microstructure during the furnace cooling or long-time isothermal holding. The above deviation suggests that the maximum carbon concentration is more than 1.5 mass% in the early austenite transformed from the cementite. For this reason, during the production of dual phase (DP) steels, a low-temperature austenitization heating is widely employed in order to get stable retained austenite with higher carbon concentration.

As is observed in ferrite lattice parameter change as a function of temperature, slight deviation from the linear line can be detected in the austenite/ferrite dual phase region, which implies the compressive internal stress really exists during the phase transformation. Therefore, the lattice parameter of austenite is influenced not only by the carbon concentration but also the tensile internal stress which is balanced with the compressive internal stress in ferrite. In Fig. 5b, the inserted data labeled "120 s step" were obtained by another experiment with faster cooling rate [13]. It is found that the rapid cooling suppresses the carbon enrichment in austenite and increases the compressive internal stress in ferrite balanced with the tensile internal stress in austenite. Accordingly, it is suspected that a larger transformation strain appears during rapider cooling such as quenching, accompanying the martensite shear transformation or non-diffusional transformation.
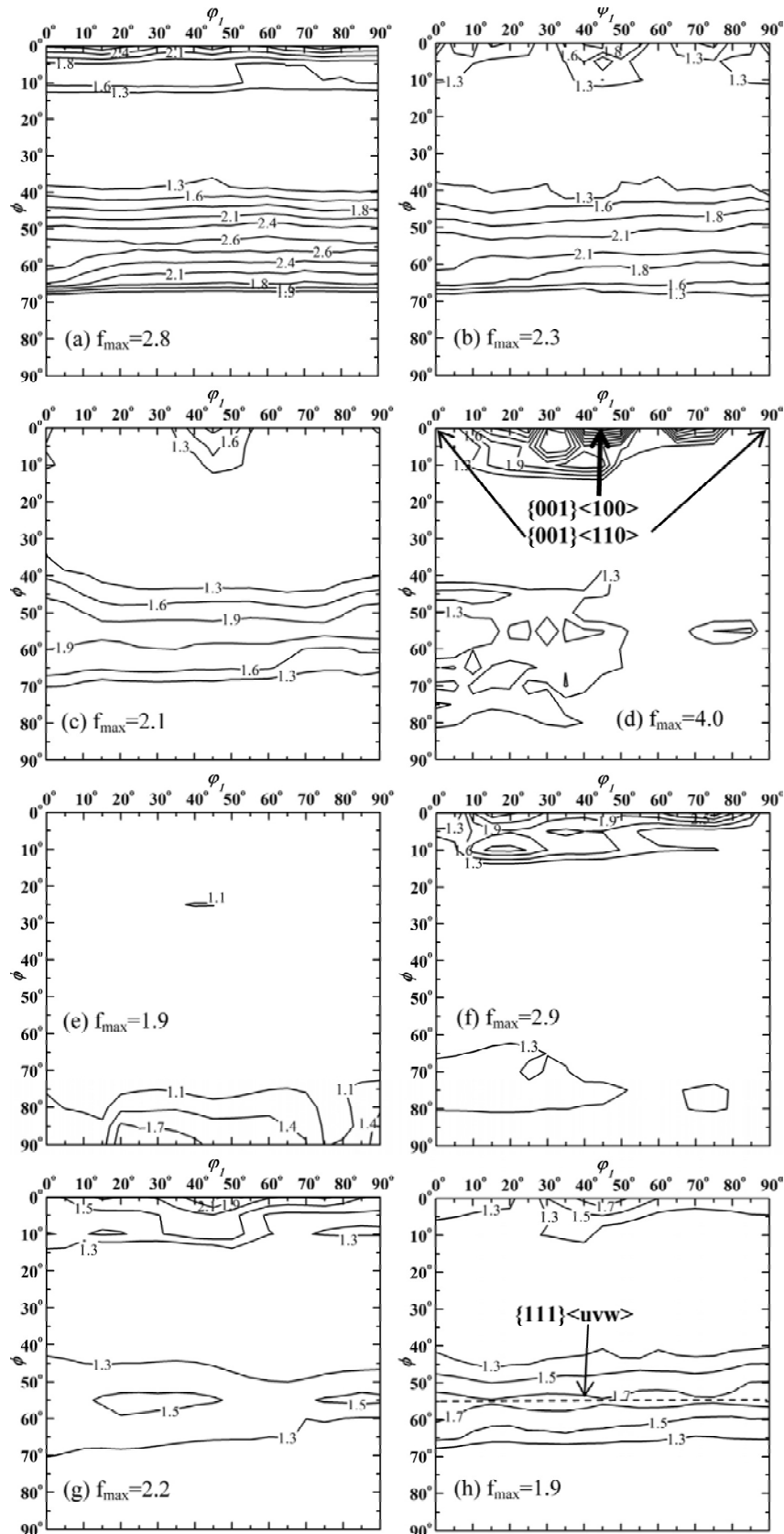
Fig. 6. Changes in φ2 = 45° ODF sections of 50% cold compressed 2Mn-0.2C steel measured by LANSCE/ HIPPO during step-by-step heating (a-e) and cooling (f-h) as shown in Fig. 1: (a) cold compressed martensite, 323K; (b) recrystallized ferrite, 873K; (c) ferrite in dual phase region, 993K; (d) ferrite in dual phase region, 1073K; (e) single phase austenite, 1173K; (f) ferrite in dual phase region, 993K; (g) ferrite in dual phase region, 913K; (h) single phase ferrite, 473K.

3.2. Texture evolution

Fig. 6 shows the texture change of cold compressed 2Mn-0.2C martensite steel with some residual hot-rolling texture characteristics obtained during the *in situ* neutron diffraction experiment with HIPPO. During heating, the {001}<110> orientation component of cold compressed martensite weakens due to the static recrystallization while the {001}<100> component shows no much change. During the ferrite-to-austenite transformation, the {111}<uvw>-fiber oriented ferrite is more favorable to transform into austenite than the {001}<100> orientation component, showing that the latter is of higher thermal stability. During cooling, the {001}<100> oriented grains are preferable to nucleate and then the {111}<uvw>-fiber oriented ferrite grains appear gradually. From Figs. 6b to 6g, it is found that the texture memory effect occurs during $\alpha \rightarrow \gamma \rightarrow \alpha$ phase transformation. However, due to the static recrystallization during heating, the cold compression texture (a) cannot be memorized. Here, the deformation stored energy obtained from cold compression is consumed during the recrystallization, and the diffusional $\alpha \rightarrow \gamma \rightarrow \alpha$ phase transformation is suspected to occur without remarkable influence from the deformation stored energy. Recently, the occurrence of texture memory effect was confirmed in the $\alpha \rightarrow \gamma \rightarrow \alpha$ phase transformation using a temperature cycle of 298K for 1.8 ks $\rightarrow$ 1148K (Ae3 = 1103K) for 1.8ks + 1.8ks $\rightarrow$ 673K for 1.8 ks though no austenite-ferrite dual phase region texture evolution was in situ observed and the initial hot-rolled texture [18] was a little different with those in this paper. These two experiments suggest that the texture memory effect is not directly related to the deformation stored energy but related to the strong variant selection and the transformation strain.

4. CONCLUSIONS

The austenite transformation, the ferrite transformation, the thermal expansion behavior and the texture evolution in a C-Mn low-alloy steel were *in situ* investigated by TOF neutron diffraction. The compressive internal strain in ferrite in ferrite/austenite dual phase region was found during both heating and cooling. The carbon enrichment and the transformation strain in austenite in a dual phase region result in the deviation of austenite lattice parameter from linear thermal expansion. The texture memory effect between the cold compression texture of the initial martensite and the final texture of ferrite after $\alpha \rightarrow \gamma \rightarrow \alpha$ phase transformation was interrupted by static recrystallization of martensite, suggesting that the texture memory effect has no direct relation to the deformation stored energy but relates to the strong variant selection and the transformation strain.

ACKNOWLEDGEMENTS

REFERENCES

[1] PH. Chapellier, R.K. Ray and J.J. Jonas // *Acta Metal. Mater.* **38** (1990) 1475.

[2] R.K. Ray and J.J. Jonas // *Int. Mater. Rev*. **35** (1990) 1.

[3] J. Savoie, R.K. Ray, M.P. Butron-Guillen and J.J. Jonas // *Acta Metal. Mater.* **42** (1994) 2511.

[4] H.-R. Wenk, I. Huensche and L. Kestens // *Metal. Mater. Trans. A.* **38** (2007) 261.

[5] M.P. Butron-Guillen, C.S. Da Costa Viana and J.J. Jonas // *Metal. Mater. Trans. A.* **28** (1997) 1755.

[6] G. Bruckner and G. Gottstein // *ISIJ Int.* **41** (2001) 468.

[7] M. Humbert, B. Gardiola, C. Esling, G. Flemming and K.E. Hensger // *Acta Mater.* **50** (2002) 1741.

[8] L. Kestens, R. Decocker and R. Petrov // *Mater. Sci. Forum* **408-412** (2002) 1173.

[9] P.G. Xu and Y. Tomota // *Acta Metall. Sinica* **42** (2006) 681.

[10] P.G. Xu, Y. Tomota and E.C. Oliver // *ISIJ Int.* **48** (2008) 1618.

[11] M. Onink, C.M. Brakman, F.D. Tichelaar, E.J. Mittemeijer and S. van der Zwaag // *Scripta Metall. Mater.* **29** (1993) 1011.

[12] S.G.E. Te Velthuis, J.H. Root, J. Sietsma, M.Th. Rekveldt and S. van der Zwaag // *Acta Mater.* **46** (1998) 5223.

[13] P.G. Xu, Y. Tomota, O. Muransky, P. Lukas and Y. Adachi // *Mater. Sci. Eng. A* **435-436** (2006) 46.

[14] T. Ohta, F. Izumi, K. Oikawa and T. Kamiyama // *Physica B (Amsterdam)* **234-236** (1997) 1093.

[15] F. Izumi and T. Ikeda // *Mater. Sci. Forum* **321-324** (2000) 198.

[16] H.-R. Wenk, L. Lutterotti and S.C. Vogel // *Nucl. Instr. and Meth. A* **515** (2003) 575.

[17] L. Lutterotti, S. Matthies, H.-R. Wenk, A.J. Schultz and J. Richardson // *J. Appl. Phys.* **81** (1997) 594.

[18] T. Tomida, M. Wakita, M. Yasuyama, S. Sugaya, M. Yonemura, Y. Tomota and S.C. Voge // *Acta Mater.* **61** (2013) 2828